

On the possible turbulence mechanism in accretion disks in non-magnetic binary stars

E. P. Kurbatov^{*1}, D. V. Bisikalo^{†1}, and P. V. Kaygorodov^{‡1}

¹Institute of Astronomy, Russian Acad. Sci.

October 1, 2014

Abstract

The arising of turbulence in gas-dynamic (non-magnetic) accretion disks is a major issue of modern astrophysics. Such accretion disks should be stable against the turbulence generation, in contradiction to observations. Searching for possible instabilities leading to the turbulization of gas-dynamic disks is one of the challenging astrophysical problems. In 2004, we showed that in accretion disks in binary stars the so-called precessional density wave forms and induces additional density and velocity gradients in the disk. Linear analysis of the fluid instability of an accretion disk in a binary system revealed that the presence of the precessional wave in the disk due to tidal interaction with the binary companion gives rise to instability of radial modes with the characteristic growth time of tenths and hundredths of the binary orbital period. The radial velocity gradient in the precessional wave is shown to be responsible for the instability. A perturbation becomes unstable if the velocity variation the perturbation wavelength scale is about or higher than the sound speed. Unstable perturbations arise in the inner part of the disk and, by propagating towards its outer edge, lead to the disk turbulence with parameters corresponding to observations (the Shakura-Sunyaev parameter $\alpha \lesssim 0.01$).

PACS numbers: 47.20.-k, 47.27.-i, 95.30.Lz

1 Introduction

High accretion rates observed in accretion disks in binary stars can be explained only by the presence of turbulent viscosity [1–3] (see also a historical review [4]). The turbulence itself should arise due to some instability [1, 3]. For a long time, attempts have been made to search for fluid instabilities in Keplerian disks (see, for example, references in paper [5]). However, it can be shown that in a Keplerian disk small radial perturbations are stable according to the Rayleigh criterion [6]. In addition, numerical simulations [6] suggest that azimuthal short wavelength modes do not display instability as well. The numerical study of long wavelength perturbations in a thin Keplerian disk [5] revealed that such perturbations grow to become non-linear and then decay not quenching the disk turbulence.

^{*}kurbatov@inasan.ru

[†]bisikalo@inasan.ru

[‡]pasha@inasan.ru

Many authors have applied the magneto-rotational instability (MRI) [7, 8] to accretion disks [9]. However, this type of instability as the reason for disk turbulence meets some difficulties: (i) in the majority of close binary stars there is no observational evidence for the magnetic field; (ii) the disk turbulence due to MRI requires the presence of a seed magnetic field; (iii) the magnetic field growth stabilizes perturbations, i.e. suppress the instability [8]; (iv) at the non-linear stage MRI saturates and, as a consequence, the angular momentum transfer through the disk significantly decreases [10]. In addition, recently the very existence of MRI in thin disks was questioned [11].

There have been several papers that further examined the fluid turbulence in the disks. For example, in paper [12] the turbulence was proposed to arise due to the super-reflection instability. Papers [13, 14] argued that disks with negative entropy gradient (in the presence of radiative cooling) can be subjected to baroclinic instability for axially non-symmetric modes. Among the recent papers on gas-dynamic turbulence in astrophysical disks we can notice paper [15], which used the statistical approach to the turbulence modeling. In such models, the field of pressure fluctuations is represented by a stochastic force in equations of motion. Due to simplicity and generality, such a source is usually modeled as a Gaussian random process that is delta-correlated in time. In our opinion, this approach may help in studying only well developed turbulence, but not the process of its arising, as claimed by the authors [15]. The reason is that this random force is not consistent with gas-dynamic equations, therefore the growth of perturbations due to this force cannot be viewed as the appearance of fluid instability.

The study of instabilities is usually carried out in the frame of certain a priori assumptions on the structure and parameters of the accretion disk. In particular, one usually assumes a near-Keplerian velocity distribution in the disk, its homogeneity in the equatorial plane, as well as circular form of the stream lines or their weak eccentricity. In fact, such idealized assumptions can be invalid already within the ‘pure’ gas-dynamic frame. For example, in paper [16] it was shown that in a viscous accretion disk, orbits of particles are unstable with respect to the eccentricity growth, so that the disk ellipticity increases. In accretion disks in binary stars specific physical conditions can occur, including shocks, tidal interaction, resonances. These features can significantly affect the gas flow, instability growth, turbulence and angular momentum transfer. In accretion disks in semi-detached binaries, steady shocks arise due to the tidal interaction with the secondary component [17–19] and the interaction of the gas stream from the inner Lagrangian point with the circumdisk halo [20–33].

Numerical simulations also revealed that the tidal interaction with the secondary component leads to arising of a specific type of waves in accretion disks — the precessional density waves [34]. Waves of this kind have spiral form and occur virtually in the entire disk. Qualitatively, such a wave can be represented as the envelope of a family of elliptical orbits precessing in a non-symmetric gravitational field [34]. The ellipticity of orbits can result from the eccentric instability which arises due to either viscous forces [16] or resonances [35]. In the last case, linear modes are excited in the disk, and the single-arm spiral with azimuthal wave number $m = 1$ has the maximum increment [35].

Stability of the disk in which the model $m = 1$, is present has been studied earlier. For example, paper [36] considered the interaction of linear perturbations with originally specified linear mode and in the approximation of large radial wave numbers. In that paper it was shown that perturbations propagating within the disk plane can be unstable, and the increment, according to the authors’ opinion, can exceed the Keplerian frequency in the disk.

The present paper is devoted to the study of instability of radial (axially symmetric) perturbations, which form in the presence of the precessional density wave, and the wave itself here is given as a numerical solution of gas-dynamic equations. That the wave is tightly wound allows us to neglect the angular dependence of all considered values for each radial direction chosen. As a result, we shall be restricted by analysis of the radial perturbation modes only.

An important feature of the precessional wave is that it represents a smooth solution, which provides fast convergence of spectral methods used in the stability analysis. The presence of gradients at the wave significantly changes the dispersion relation for linear perturbations and leads to conditions facilitating the instability growth.

In Section 2 a scenario of the density wave arising is presented. In Section 3 the linear analysis of perturbations in a thin isothermal Keplerian disk is introduced and applied to the numerical model of the accretion disk with precessional wave. In Section 4, a physical analysis of the results is performed. The discussion of results and conclusion are given in Section 5.

2 Precessional density wave

Accretion disks in semi-detached binaries have a sufficiently complicated structure, since the tidal forces and the disk interaction with the inter-component envelope and the gas stream from the inner Lagrangian point L_1 deform the disk shape and lead to the formation of different shocks. Tidal shocks and the ‘hot line’ — the region of impact of the gas stream from the inner Lagrangian point L_1 with the circumdisk halo — mostly affect the flow. Three-dimensional hydrodynamic simulations demonstrate that these waves do not penetrate deep inside the cold (with a temperature of $\sim 10^4$ K) accretion disk and leave most of the disk weakly perturbed, which creates conditions for the third-type wave, the precessional density wave, to appear [34]. The form of stream lines in the accretion disk is close to the corresponding elliptical Keplerian orbits with the accreting star residing in one of the focuses. This can be explained by the fact that in the region free from strong gas-dynamic perturbations due to steady shocks, the disk is almost homogeneous and gravitational forces dominate over forces due to gas pressure gradients in the equatorial plane of the system. The tidal interaction increases the stream line eccentricity in the disk and forces their apse line to counter rotate the disk. The tidal forces act on the stream lines non-homogeneously: the outer stream lines tend to rotate faster than the inner ones, since in a gas disk (at least if the Knudsen number¹ is much less than one) there can be no intersecting stream lines, some mean precessional velocity is established, which is one and the same for all stream lines. This velocity can be approximately estimated using the formula [37, 38]:

$$\frac{P_{\text{pr}}}{P_{\text{orb}}} \simeq \frac{4}{3} \frac{(1+q)^{1/2}}{q} \left(\frac{r}{A}\right)^{-3/2}, \quad (1)$$

where P_{pr} is the precessional period; P_{orb} is the system’s orbital period; q is the binary components mass ratio; r is the characteristic size of the orbit; A is the distance between the binary components.

The approaching of stream lines that moves with different velocities leads to the formation of a spiral pattern shown schematically in Fig. 1. The matter velocity along the stream line, whose form is primarily determined by gravitation, will be close to the local Keplerian velocity for the corresponding (elliptical) orbit. Accordingly, the velocity will be minimal at the stream line apastron. However, as the flux value should be conserved along the stream line, the matter density should also change along the stream line and reach maximum at the apastron. Therefore, the spiral arm formed by the stream lines apastrons will look like the density wave, as was shown in paper [34].

In the observer’s reference frame the precessional wave is almost steady — its shifts by $1^\circ - 3^\circ$ in the retrograde direction in one orbital period [34]. Thus, the density and velocity

¹The Knudsen number here is the ratio of the particle free-path length to the characteristic scale of the problem, which here can be the disk thickness. For the typical number density in the accretion disk of the order of 10^{11} cm^{-3} the free path length is 10^{-10} a.u., while the disk thickness is $\lesssim 10^{-2}$ a.u.

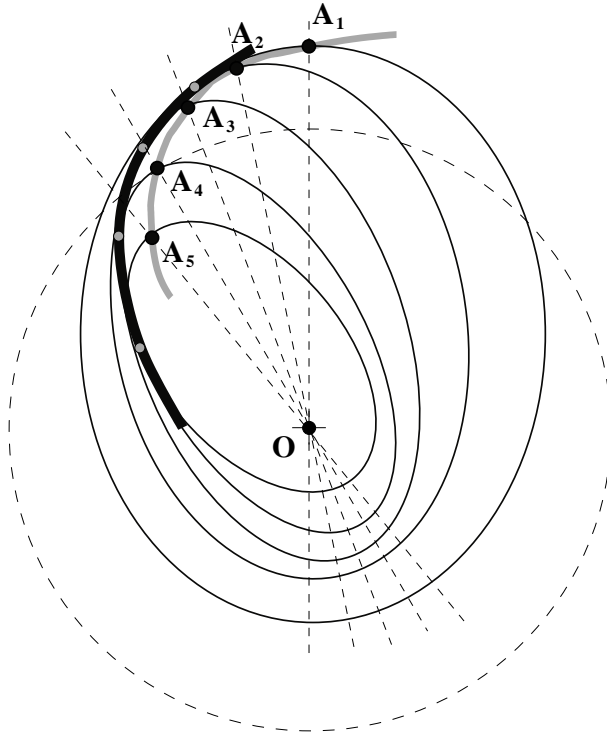


Figure 1: Schematics of the spiral pattern formation in the inner unperturbed parts of cold gas disks. The accretor is at the center (O), $A_1 \dots A_5$ denote the stream line apastrons.

distribution in the wave can be considered stationary on time scales of the order of several tens of the characteristic disk periods.

Fig. 2 shows distributions of the surface density and the radial and angular velocity in the numerical simulations of the disk in a close binary system [34]. The calculations were carried out for the binary with parameters: accretor's mass $M_1 = 1 M_\odot$, donor's mass $M_2 = 0.05 M_\odot$, binary separation $A = 0.625 R_\odot$, binary orbital period $P_{\text{orb}} = 4830$ s. The precessional wave is distinctly seen as a spiral-like overdensity in the surface density map. In the radial velocity map the region with the density wave is bounded by the zero radial velocity lines. The zero tangential velocity lines coincide with radial velocity extrema.

The surface density, radial and tangential velocity distributions are shown in Fig. 3 along four radial directions in the disk: 180° , 225° , 270° , and 315° (0° corresponds to the direction from the secondary component along the line connecting the binary components centers). The density peaks observed at phases $0.15 - 0.25$ correspond to intersections of the profiles with the precessional wave and well correlate with the radial velocity minima. The radial and tangential velocity profiles are significantly different along different directions. Nevertheless, these profiles share common features determined by properties of elliptical orbits. For example, for all profiles the tangential velocity is, on average, sub-Keplerian (as accretion occurs through the disk), however in the outer parts of the disk the tangential velocity is much smaller than in the inner parts, since the velocity of matter moving along a Keplerian orbit decreases with distance from the star. The radial velocity distribution significantly depends on the direction — three profiles presented in Fig. 3b demonstrate positive (i.e. directed away from the accretor) velocity in the inner parts of the disk, at the same time the radial velocity in the fourth profile is negative in the same region. This behavior is clear, since the matter moving along an eccentric orbit can be closer to or further away from the star at different parts of the trajectory. Nevertheless, it should be noted that in the outer parts of the disk the radial velocity is positive for all profiles, since the angular momentum of the disk decreases in the outer parts due to decretion of matter. It should be specially stressed that the radial velocity difference over the disk is fairly large and

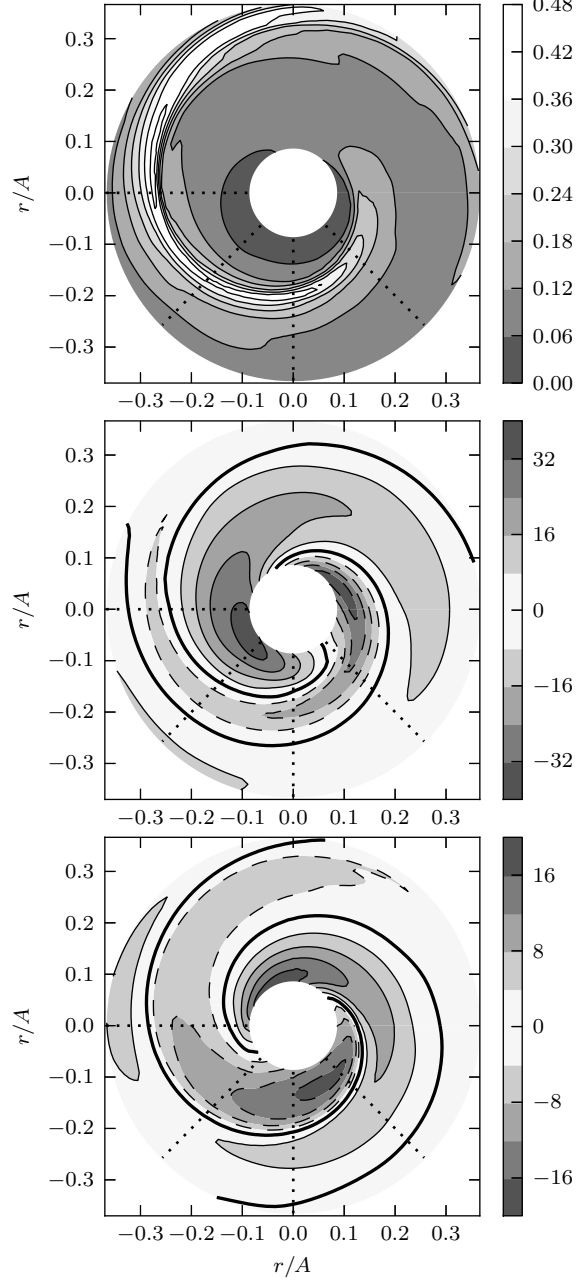


Figure 2: Maps of the surface density (upper panel), radial velocity (middle panel) and deviations of the angular velocity from the Keplerian profile (bottom panel) according to the numerical model [34]. Velocities are in units of the sound speed c_T . The thick lines show zero velocity levels.

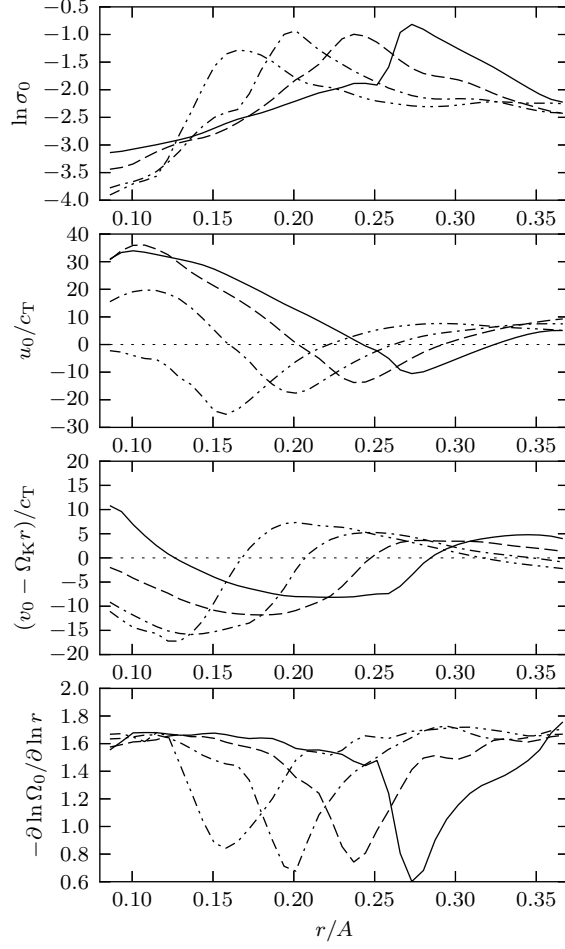


Figure 3: Plots of the surface density (a), radial velocity (b), angular velocity (c) and the rotational curve slope (d) in the numerical accretion disk model [34]. The plots correspond to the radial disk cuts in the directions 180° (the solid curves), 225° (the dashed curves), 270° (the dash-dotted curves) and 315° (the dash-double-dotted curves).

along some directions can be as large as several tens of sound speed.

As follows from the distributions presented in Fig. 2, the precessional wave is tightly wounded. This allows one approximately treat perturbations caused by the wave as axially symmetric. This approximation cannot be valid in the central parts of the disk, where the axial symmetry is significantly violated (it is the most clearly seen in the velocity distribution). In what follows, we shall analyze perturbations excluding the central part of the disk with radius smaller than $0.08 A$ from calculations. The results of calculations suggest that the outer parts of the disk are subjected to strong gas-dynamic perturbations. At shocks located close to the disk edge, the stream lines are broken, and correspondingly the methods we use in the present paper cannot be applied to study instabilities in these regions, since the calculation domain was limited by the radius $0.37 A$.

3 Linear analysis of perturbations in a disk with precessional wave

The density and radial and tangential velocity distributions obtained in the numerical simulations [34], which were described in Section 2, were taken as the background distributions for the analysis of perturbations. Perturbations propagating in the direction perpendicular to the disk are sound perturbations, i.e. they do not show instability. Therefore, it seems plausible to assume that the account for vertical perturbations can lead to the appearance of additional sound modes and only insignificantly change frequencies and increments of radial perturbations. These considerations allow significant simplifications of calculations to be made by excluding the vertical degree of freedom. All the subsequent analysis is carried out in two dimensions. Therefore, the results of numerical simulations were reduced to two dimensions by integrating distributions along the direction perpendicular to the disk [39].

The calculations were performed in the inertial reference frame, where the precessional wave is almost at rest. The presence of the time-dependent gravitational field of the secondary component in this frame, generally speaking, can give rise to additional spiral pattern co-moving with the rotation [40]. The amplitude of deviations in the density and radial and tangential velocity distributions due to this effect is scaled with the components mass ratio [40], which in our case is very small. Thus, we assume that the gas distribution in the inertial reference frame is steady.

3.1 Approach

We shall use the isothermal thin disk approximation in two dimensions. This approximation is quite adequate to accretion disks in binary systems, since the effective temperature is of the order of 10^4 K and the characteristic ratio of the disk thickness to its radius for this temperature is $\lesssim 0.01$. The two-dimensional disk flow in the (r, ϕ) plane is obtained by integrating the complete system of gas-dynamic equations along the vertical coordinate z . The parameters of this system include the surface density $\sigma = \int dz \rho$, the radial and angular velocities u and $v = \Omega r$, as well as the flat pressure $p = \int dz P$, where ρ , P are the volume density and pressure, respectively. For a perfect gas with the adiabatic index γ , the flat pressure is a power law of the surface density with the ‘adiabatic index’ $\gamma_S = 1 + 2(\gamma - 1)/(\gamma + 1)$ [39, 41–43]. However, in the isothermal case $\gamma_S = 1$ [39, 42] and the flat pressure will have the same form as the volume pressure, $p = c_T^2 \sigma$. The correct reduction of the system of three-dimensional equations to two dimensions, generally speaking, gives rise to additional terms in equations compared to

the three-dimensional form [39, 42]. The initial two-dimensional system reads:

$$\frac{\partial \sigma}{\partial t} + \nabla(\sigma \mathbf{V}) = 0, \quad (2)$$

$$\frac{\partial \mathbf{V}}{\partial t} + (\mathbf{V} \nabla) \mathbf{V} = -\nabla \Phi_1 - \nabla \Phi_2 - c_T^2 \nabla \ln(\Omega_K \sigma). \quad (3)$$

Here σ is the surface density; $\mathbf{V} = \mathbf{e}_r u + \mathbf{e}_\phi v$; $\Phi_1 = -GM_1/r$, $\Phi_2 = -GM_2/|\mathbf{R}_1 - \mathbf{R}_2 + \mathbf{r}|$ are gravitational potentials of the accretor and donor, respectively; c_T is the sound speed; $\mathbf{R}_1, \mathbf{R}_2$ are radius-vectors from the barycenter to the accretor and donor, respectively; $\Omega_K = (GM_1/r^3)^{1/2}$ is the Keplerian angular velocity; G is the gravitational constant.

As the adopted mass ratio M_2/M_1 is small, the binary system barycenter lies close to the accretor. We will assume accretor's center at the barycenter: $R_1 \approx 0$, $R_2 \approx A$. We also denote $M \equiv M_1$, $q \equiv M_2/M_1$. In the cylindrical coordinates we obtain:

$$\frac{\partial \sigma}{\partial t} + \frac{1}{r} \frac{\partial(r\sigma u)}{\partial r} + \frac{1}{r} \frac{\partial(\sigma v)}{\partial \phi} = 0, \quad (4)$$

$$\frac{\partial u}{\partial t} + u \frac{\partial u}{\partial r} + \frac{v}{r} \frac{\partial u}{\partial \phi} - \frac{v^2}{r} = -\frac{GM}{r^2} - \frac{qGM(A \cos \phi + r)}{(A^2 + r^2 + 2Ar \cos \phi)^{3/2}} - c_T^2 \frac{\partial \ln(\Omega_K \sigma)}{\partial r}, \quad (5)$$

$$\frac{\partial v}{\partial t} + u \frac{\partial v}{\partial r} + \frac{v}{r} \frac{\partial v}{\partial \phi} + \frac{uv}{r} = -\frac{c_T^2}{r} \frac{\partial \ln \sigma}{\partial \phi} + \frac{qGMA \sin \phi}{(A^2 + r^2 + 2Ar \cos \phi)^{3/2}}. \quad (6)$$

Here ϕ is the azimuthal angle in the disk, $\phi = 0$ corresponds to the direction towards the secondary companion along the line connecting the centers of the binary components.

Let us set small perturbations and linearize the equations. The disk model with precessional wave (see Section 2). will be taken as the unperturbed solution. The perturbations can be written in the form: $\sigma \mapsto \sigma_0(1 + \delta)$, $u \mapsto u_0 + u$, $v \mapsto \Omega_0 r + v$, where $|\delta| \ll 1$, $|u| \ll |u_0|$ and $|v| \ll |\Omega_0 r|$; the values σ_0 , u_0 and Ω_0 correspond to the unperturbed solution. Linearization of the equations results in disappearing of terms responsible for gravitational interaction with the donor. Equations for perturbations take the form

$$\frac{\partial \delta}{\partial t} + u_0 \frac{\partial \delta}{\partial r} + \Omega_0 \frac{\partial \delta}{\partial \phi} + \frac{\partial u}{\partial r} + \left(\frac{\partial \ln \sigma_0}{\partial r} + \frac{1}{r} \right) u + \frac{1}{r} \frac{\partial v}{\partial \phi} + \frac{1}{r} \frac{\partial \ln \sigma_0}{\partial \phi} v = 0, \quad (7)$$

$$\frac{\partial u}{\partial t} + u_0 \frac{\partial u}{\partial r} + \Omega_0 \frac{\partial u}{\partial \phi} + \frac{\partial u_0}{\partial r} u + \left(\frac{1}{r} \frac{\partial u_0}{\partial \phi} - 2\Omega_0 \right) v + c_T^2 \frac{\partial \delta}{\partial r} = 0, \quad (8)$$

$$\frac{\partial v}{\partial t} + u_0 \frac{\partial v}{\partial r} + \Omega_0 \frac{\partial v}{\partial \phi} + \left(\frac{u_0}{r} + \frac{\partial \Omega_0}{\partial \phi} \right) v + \frac{\varkappa_0^2}{2\Omega_0} u + \frac{c_T^2}{r} \frac{\partial \delta}{\partial \phi} = 0. \quad (9)$$

Here \varkappa_0^2 is the square of the epicyclic frequency

$$\varkappa_0^2 = 2\Omega_0 \left(2\Omega_0 + r \frac{d\Omega_0}{dr} \right). \quad (10)$$

Let us express perturbations in terms of harmonics $f_\alpha(t, r, \phi) \mapsto e^{-i\omega t} f_\alpha(r, \phi)$, where $(f_\alpha) = [\delta, u, v]$, then the system of equations (7–9) can be represented in the matrix form

$$\sum_{\beta=1}^3 A_{\alpha\beta}(r, \phi) f_\beta(r, \phi) = i\omega f_\alpha(r, \phi). \quad (11)$$

The characteristic scale of variations of the background variables along the radius is about $0.1A$ (see Fig. 3), and along the angular coordinate is about $2\pi r$. Thus, at $r \gg 0.016A$ the angular dependence of the background variables can be neglected. Then the problem

splits in two independent one-dimensional problems, and the density and velocity along the corresponding radial direction in the disk can be taken as unperturbed solutions of each of them. Assuming that the perturbations are also independent of the angle, we obtain the system of equations for radial perturbations (see Appendix A):

$$\sum_{\beta=1}^3 A_{\alpha\beta}(r) f_{\beta}(r) = i\omega f_{\alpha}(r) , \quad (12)$$

where the matrix of the operator $A_{\alpha\beta}$ has the form

$$\begin{bmatrix} u_0 \frac{d}{dr} & \frac{d \ln \sigma_0}{dr} + \frac{1}{r} + \frac{d}{dr} & 0 \\ c_T^2 \frac{d}{dr} & \frac{du_0}{dr} + u_0 \frac{d}{dr} & -2\Omega_0 \\ 0 & \frac{\varkappa_0^2}{2\Omega_0} & \frac{u_0}{r} + u_0 \frac{d}{dr} \end{bmatrix} \quad (13)$$

The values $i\omega$ are eigenvalues of the operator $A_{\alpha\beta}$, and its eigenfunctions are the solution f_{α} of the system. Thus, equation (12) is a Sturm-Liouville problem.

As the unperturbed solution is sufficiently smooth, as well as to avoid differentiation with respect to radius, we shall solve equation (12) by the Galerkin method in some functional basis representation. The problem geometry suggests that the zero-order Bessel functions of the first kind can be conveniently chosen as the new functional basis. In the present paper the unperturbed disk state is specified by the numerical solution on the discrete space grid, so we use the discrete Hankel transform for the Bessel functions in the form [44]:

$$\hat{f}_{\alpha}(k_p) = \sum_{q=1}^N \frac{2J_0(k_p r_q)}{\mu_{N+1}^2 J_1^2(\mu_q)} f_{\alpha}(r_q) , \quad (14)$$

$$f_{\alpha}(r_q) = \sum_{p=1}^N \frac{2J_0(k_p r_q)}{\mu_{N+1}^2 J_1^2(\mu_p)} \hat{f}_{\alpha}(k_p) , \quad (15)$$

where μ_q is the q -th root of the function J_0 ; N is the dimension of the spatial grid. This transform assumes that the function $f(r)$ is given at the finite interval $0 \leq r \leq R$ and vanishes at the interval boundary. Its values should be calculated at the points $r_q = R\mu_q/\mu_{N+1}$. The values of the image $\hat{f}(k_p)$ should be calculated at points $k_p = \mu_p/R$.

Equation (12) can be recast to the form

$$\sum_{s=1}^N \sum_{\beta=1}^3 \hat{A}_{\alpha\beta}(k_p, k_s) \hat{f}_{\beta}(k_s) = i\omega \hat{f}_{\alpha}(k_p) , \quad (16)$$

where

$$\hat{A}_{\alpha\beta}(k_p, k_s) = \frac{4}{\mu_{N+1}^4} \sum_{q=1}^N \frac{J_0(k_p r_q)}{J_1^2(\mu_q)} A_{\alpha\beta}(r_q) \frac{J_0(k_s r_q)}{J_1^2(\mu_q)} . \quad (17)$$

Note that the differential operator of the form $g(r) d/dr$ for an arbitrary function should be transformed as

$$g(r) \frac{d}{dr} \mapsto \frac{4}{\mu_{N+1}^4} \sum_{q=1}^N \frac{J_0(k_p r_q)}{J_1^2(\mu_q)} \frac{k_s}{2} \frac{J_{-1}(k_s r_q) - J_1(k_s r_q)}{J_1^2(\mu_q)} g(r_q) . \quad (18)$$

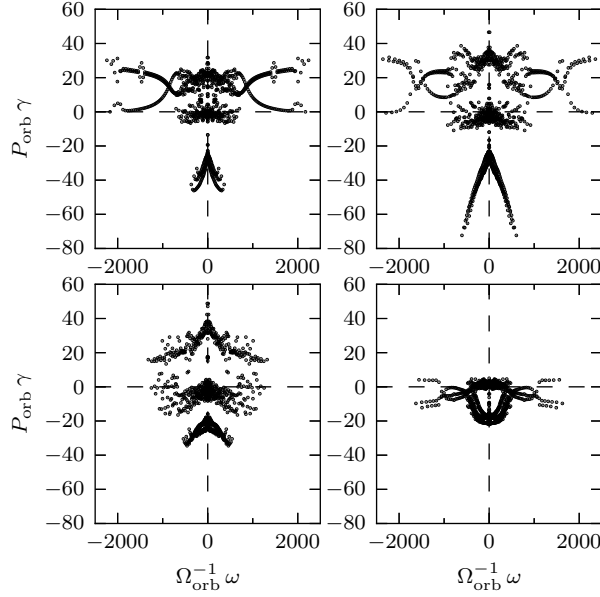


Figure 4: Maps of complex frequencies of eigensolutions in the disk cuts from Fig. 3.

Finally, to reduce the system of algebraic equations (16) to the suitable form to which known methods of solving the eigenvalue problem can be applied, we linearly compose elements of the vector $\hat{f}_\alpha(k_p)$ as follows:

$$(\hat{f}_I) = \left[\hat{f}_1(k_1), \hat{f}_2(k_1), \hat{f}_3(k_1), \hat{f}_1(k_2), \hat{f}_2(k_2), \hat{f}_3(k_2), \dots \right]. \quad (19)$$

In a similar way we compose the matrix \hat{A}_{IJ} to finally obtain

$$\sum_{J=1}^{3N} \hat{A}_{IJ} \hat{f}_J = i\omega \hat{f}_I. \quad (20)$$

Eigenvalues of the matrix \hat{A}_{IJ} give the spectrum of angular frequencies of possible solutions, and eigenvectors give the solution in the Bessel functions representation. For the given spatial grid dimension N we have $3N$ complex eigenfrequencies and N eigenvectors for each field (δ , u or v).

3.2 Calculation

The method described in Section 3.1 can be used to calculate linear perturbations on the axially symmetric backgrounds. In the frame of the numerical model of accretion disk considered in Section 2, this assumption, strictly speaking, is invalid. However, it is possible to state that for each radial direction the angular dependence of all variables is small, and therefore each radial distribution can be considered axially symmetric. In our problem this method was independently applied to each radial cut of the disk. The parameters of the method include: the computational domain size $0.08 A \leq r \leq R = 0.37 A$, the grid dimension $N = 439$. Equation (20) was solved using the LAPACK library [45].

The maps of complex frequencies for all perturbation modes are presented in Fig. 4. The maximum absolute values of angular frequencies in calculations reach $1500 \Omega_{\text{orb}}$, and therefore the increments lie within the range from $-70 P_{\text{orb}}$ to $50 P_{\text{orb}}$. The minimal perturbation length for the given grid dimension N is around $\lambda_N \equiv 2R/N \approx 3 \cdot 10^{-3} A$. This wavelength can be compared to the Keplerian angular frequency $(GM/\lambda_N^3)^{1/2} \approx 6 \cdot 10^3 \Omega_{\text{orb}}$, whereas the

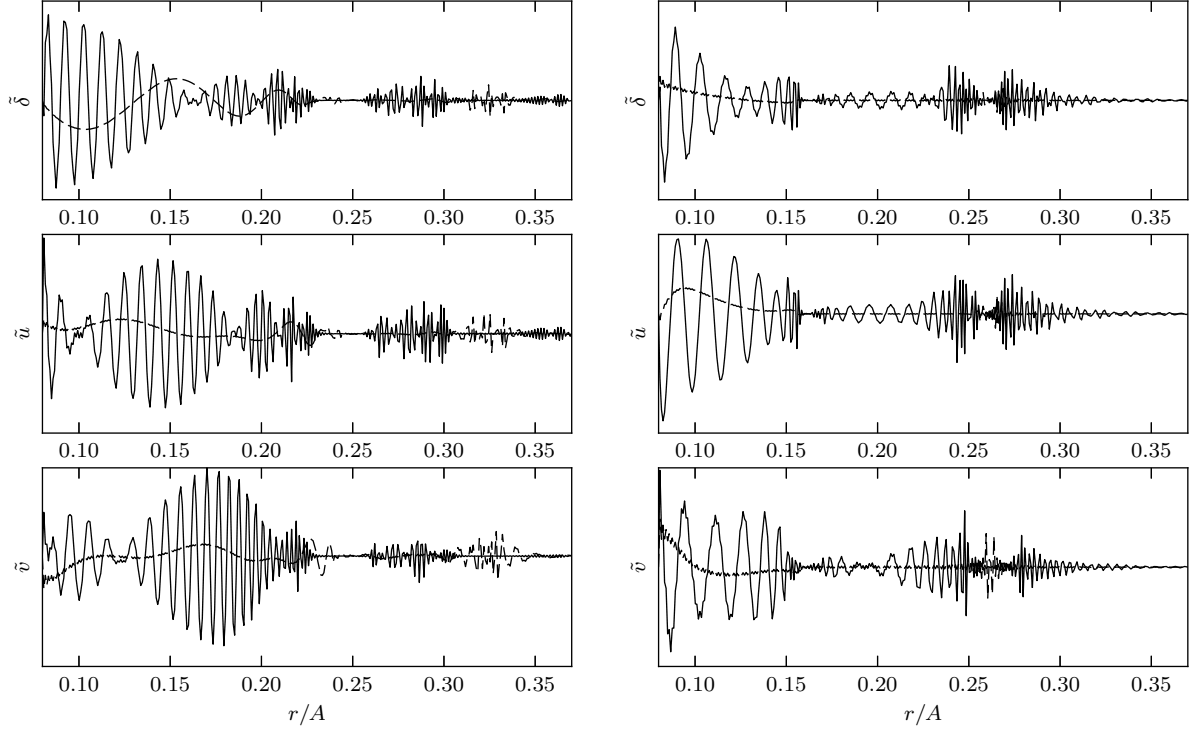


Figure 5: Real parts of the complex solutions for density, radial and angular velocity perturbations for some modes in the cuts (see Fig. 3) corresponding to 180° (left panels) and 270° (right panels). Left plots correspond to $\omega = 379.6 \Omega_{\text{orb}}$, $\gamma = 22.3/P_{\text{orb}}$ (the solid curves) and $\omega = 35.2 \Omega_{\text{orb}}$, $\gamma = 22.6/P_{\text{orb}}$ (the dashed curves). Right plots to $\omega = 158.0 \Omega_{\text{orb}}$, $\gamma = 25.7/P_{\text{orb}}$ (the solid curves) and $\omega = 10.4 \Omega_{\text{orb}}$, $\gamma = 48.8/P_{\text{orb}}$ (the dashed curves).

corresponding sound frequency is $2\pi c_T/\lambda_N \approx 40 \Omega_{\text{orb}}$. Note that these estimates depend on the spatial discretization scale. This scale can be related to the maximum and minimum angular frequencies obtained in calculations.

As the original unperturbed solution is inhomogeneous, the perturbation amplitude is different at different points of the disk. The rate of growth or decay of perturbations is determined both by the imaginary part of the eigenfrequency and by its local amplitude. Fig. 5 shows real parts of eigenvectors for some modes in two cuts of the disk corresponding to 180° and 270° (imaginary parts of the solutions are different from real parts only by spatial phase).

Eigenvectors can have inhomogeneous spectral composition – the local wavelength, being defined as the distance between maxima in different parts of the disk, can differ by many times (see Fig. 4). When examining the spectral composition of the solutions in different parts of the disk, the wavelet-analysis may be helpful. For each mode, let us calculate the deconvolution²

$$w(r, \lambda) = \int dr' |W(r - r', \lambda) \delta(r')| , \quad (21)$$

where W is the Morlet wavelet [47] of order 5,

$$W(r, \lambda) = \exp \left[-\frac{1}{2} \left(\frac{2\pi}{5} \frac{r}{\lambda} - 2\pi \right)^2 \right] \exp \left(i2\pi \frac{r}{\lambda} \right) . \quad (22)$$

The distribution of $w(r, \lambda)$ over wavelengths shows the characteristic scale of change of λ dominating around given r .

²In the cylindrical coordinates, the Morlet wavelet and this type of transform are, strictly speaking, inapplicable [46], but for approximate accuracy estimates this transform turns out to be sufficient.

The turbulence viscosity coefficient ν_{turb} or related to it the Shakura-Sunyaev parameter $\alpha = \nu_{\text{turb}}/(c_T h)$, where $h = c_T/\Omega_K$ is the semi-thickness of the Keplerian disk! [2], is the commonly accepted characteristic of the efficiency of the angular momentum transfer in accretion disks. Although ν_{turb} is pertinent to well developed turbulence, in paper [48] its relation to the characteristics of unstable liner perturbations was obtained:

$$\nu_{\text{turb}} = \frac{\gamma \lambda^2}{4\pi^2}, \quad (23)$$

where λ and γ are the maximum wavelength and maximum increment for all growing modes for a given type (given branch) of perturbations. A similar approach to the turbulent viscosity estimate was proposed in paper [12] based on plasma theory results [49, c. 299], where the instability was considered as a consequence of the background inhomogeneity only.

On the eigenfrequency maps (see Fig. 4) it is difficult to uniquely find perturbation branches. The estimate of ν_{turb} using maximum increments for all modes appears to be senseless because the modes with maximum increments and frequencies may reflect the spatial discretization and boundary effects. Therefore, the values of the coefficient ν_{turb} defined by formula (23) should characterize not the whole set of eigenvectors, but an individual mode at each point of the disk. This approach corresponds to general equation (7) from paper [48]. In our setting, for the mode with increment γ and the local wavelength λ we have

$$\alpha = 0.21 P_{\text{orb}} \gamma \frac{(\lambda/A)^2}{h/A}. \quad (24)$$

to describe a more or less realistic accretion disk, one should specify the power density of the family of modes and to calculate the Shakura-Sunyaev parameter as an average over the mode ensemble. For example, in paper [6] the initial conditions for the evolution of plane waves in the outer part of an accretion disk were chosen as a power-law power density spectrum (quadratic in the wave number) exponentially decaying at short wavelengths. In the present problem, the plane-wavelength approximation is invalid because the wavelength is the local variable for each mode. The statistical weight in the mode ensemble can be specified from the following considerations. Expression (23) is applicable to accretion disks with taking into account two physical conditions: (i) only three-dimensional turbulence can be induced; (ii) the characteristic growth time of a perturbation cannot exceed one disk revolution period. These conditions suggest two local restrictions — on the wavelength and increment of a perturbation:

$$\lambda \leq h, \quad \gamma \geq \frac{\Omega_0}{2\pi}. \quad (25)$$

The final expression for the Shakura-Sunyaev parameter can be written in the form

$$\alpha_k(r) = \frac{\int' d\lambda w_k(r, \lambda) \alpha_k(r, \lambda)}{\int' d\lambda w_k(r, \lambda)}, \quad (26)$$

for the mode with number k at the point r and

$$\alpha(r) = \frac{\sum_k' w_k(r) \alpha_k(r)}{\sum_k' w_k(r)}, \quad (27)$$

for all modes at the point r . The local amplitude of perturbations for all modes reads:

$$w(r) = \sum_k' \int' d\lambda w_k(r, \lambda). \quad (28)$$

Primes over the integral and sum mean that the summation is performed over the modes and wavelengths for which conditions (25) are fulfilled. The results of calculations are presented in Fig. 6.

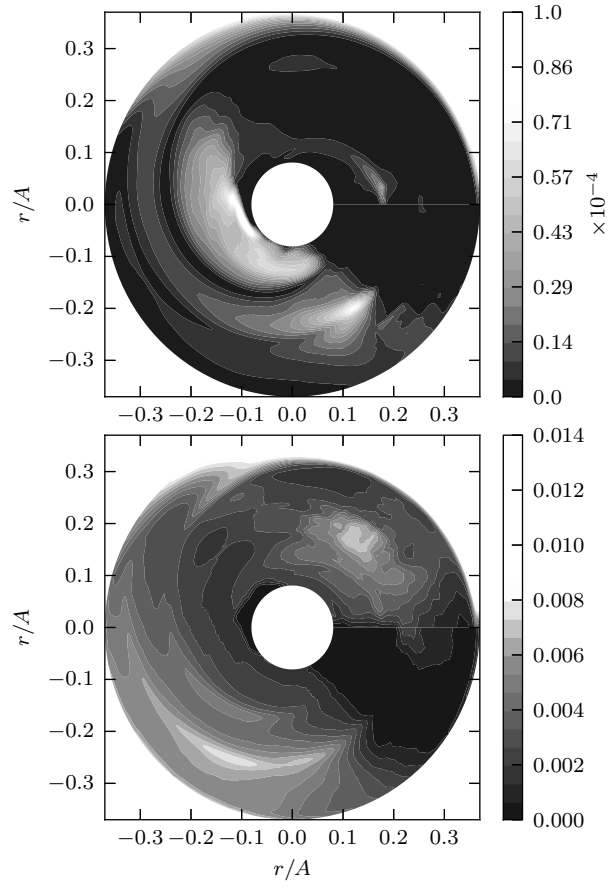


Figure 6: Perturbation amplitudes (upper panel) and the Shakura-Sunyaev parameter α (bottom panel) in the disk.

4 Physical analysis of the results

The comparison of the unperturbed distributions (see Fig. 2 and 3) with perturbation profiles (see Fig. 4) reveals several features. At first, near zeros of the function u_0 the local wave of perturbations decreases. At second, immediately near these points the local amplitude of perturbations tends to zero. The first effect can be easily explained by the following considerations. Let us maximum simplify the problem and consider the advection part of linearized equation (7):

$$\frac{\partial \delta}{\partial t} + u_0 \frac{\partial \delta}{\partial r} = 0. \quad (29)$$

The direct substitution shows that near the root r_* the function u_0 will have the form

$$\delta = \exp \left(i\omega \int \frac{dr}{u_0} - i\omega t \right). \quad (30)$$

By setting the velocity variation law as $u_0 \propto r - r_*$, we obtain that the local perturbation wavelength (defined as λ in the expression $\omega \int_r^{r+\lambda} dr/u_0 = 2\pi$) in the vicinity of r_* behaves as $\mathcal{O}(r - r_*)$.

In the immediate vicinity of zero of the function u_0 in equation (7) the divergence term becomes important. Let us write equations (7) and (8) by ignoring geometrical terms and the tangential velocity:

$$\frac{\partial \delta}{\partial t} + u_0 \frac{\partial \delta}{\partial r} + \frac{\partial u}{\partial r} = 0, \quad (31)$$

$$\frac{\partial u}{\partial t} + u_0 \frac{\partial u}{\partial r} + \frac{\partial u_0}{\partial r} u + c_T^2 \frac{\partial \delta}{\partial r} = 0. \quad (32)$$

For the background velocity variation law $u_0 \propto r - r_*$, in the limit $u_0 \ll c_T$ it is easy to show (by differentiating the Euler equation with respect to radius and by excluding velocity perturbations) that solutions take the form $\delta \propto e^{-i\omega t}(r - r_*)$ and $u \propto e^{-i\omega t}(r - r_*)^2$ such that in the immediate vicinity of the point r_* the perturbation amplitude decreases and the spatial oscillations become ‘frozen’.

Fig. 6 demonstrates that the perturbation amplitude reaches maximum in the inner part of the disk restricted by the precessional wave, while the turbulence (assumed as large values of α) is strongest in the outer part of the disk. This is most clearly seen in the second and third quadrants of the disk, where the location of the amplitude maximum coincides with the radial velocity maximum (see Fig. 2). The perturbation amplitude decreases with decreasing velocity. In the region restricted by the zero radial velocity, some amplitude growth is observed, especially close to the outer edge of the precessional wave. In the fourth quadrant, where the radial velocity in the inner part of the disk is negative (see also Fig. 3), perturbations and turbulence are almost absent, but there is an amplitude peak at the outer edge of the wave.

This behavior of the amplitude can be explained as follows. Let us utilize equations (7–9) in the simulation box approximation whose sizes are much smaller than the distance from the box to the center, like in paper [6]. Let us represent perturbations in the form $e^{-i\omega t + ikr}$ and assume that the perturbation length is sufficiently small to consider all unperturbed variables as constants, as well as to neglect geometrical terms. We obtain the equations in the form

$$(-i\omega + iku_0) \delta + \left(\frac{\partial \ln \sigma_0}{\partial r} + ik \right) u = 0, \quad (33)$$

$$ic_T^2 k \delta + \left(-i\omega + iku_0 + \frac{\partial u_0}{\partial r} \right) u - 2\Omega_0 v = 0, \quad (34)$$

$$(2 - q) \Omega_0 u + (-i\omega + iku_0) v = 0. \quad (35)$$

The epicyclic term in the angular momentum conservation law is written as $\varkappa_0^2/(2\Omega_0) \approx (2 - q)\Omega_0$, where $q \equiv -\partial \ln \Omega_0 / \partial \ln r$ [6]. The dispersion relation for this system reads:

$$\omega_{\pm} = u_0 k - \frac{i}{2} \frac{\partial u_0}{\partial r} \pm \left[c_T^2 k^2 - \frac{1}{4} \left(\frac{\partial u_0}{\partial r} \right)^2 + 2(2 - q) \Omega_0^2 - i c_T^2 \frac{\partial \ln \sigma_0}{\partial r} k \right]^{1/2}. \quad (36)$$

The second term on the r.h.s. of (36) is the divergence term that stabilizes or destabilizes perturbations depending on whether the flow is divergent ($\partial u_0 / \partial r > 0$) as in the outer part of the disk, or convergent ($\partial u_0 / \partial r < 0$) as in the inner part of the disk. The second term under the square root helps destabilizing the flow — if the radial velocity gradient is strong enough, the perturbation phases over the one-wavelength interval outrace each other. The third term under the square root in the case of zero gradients would correspond to the Rayleigh stability criterion [6] — a flow in which the logarithmic slope of the angular velocity profile $q > 2$ is unstable. Finally, the last term contributes to the instability increment at all wave numbers.

Let us evaluate each term in the dispersion equation (36) using conditions (25) and Fig. 3. The minimum local wave number at a given radius must be determined by the disk semi-thickness: $|A k_{\min}|^2 \equiv (2\pi A \Omega_K / c_T)^2 \approx 10^5 (A/r)^3$, here everywhere but in the vicinity of roots of the radial velocity, $|c_T k_{\min}| \ll |u_0 k_{\min}|$. The term with the velocity gradient turns out of the same order: $|\partial(u_0/c_T)/\partial(r/A)|^2 \lesssim 10^5$. The term corresponding to the Rayleigh criterion can be estimated as follows. The slope of the rotational curve can be assumed Keplerian everywhere (see Fig. 3), $q = 3/2$, then $2(2 - q)(A\Omega_0/c_T)^2 \approx 10^3 (A/r)^3$. It is seen that this term introduces only small stabilizing effect. The density gradient can be estimated as $|A^2 k_{\min} \partial \ln \sigma_0 / \partial r| \approx 5 \cdot 10^3 (A/r)^{3/2}$. Thus, the instability, at least in the simulation box approximation, can be only due to the radial velocity gradient. The rotational motion of the gas has only slightly stabilizing effect. The dispersion equation (36) as a result should have the form

$$\omega_{\pm} = u_0 k \pm \left[c_T^2 k^2 - \frac{1}{4} \left(\frac{\partial u_0}{\partial r} \right)^2 + 2(2 - q) \Omega_0^2 \right]^{1/2}. \quad (37)$$

Above estimates suggest that the disk is in the boundary state between the stability and instability. To clarify this point, we use the general integral method of the stability analysis described in paper [50]. In this method, gas-dynamic equations are formed through the displacement vector of gas element and the analysis assumes this displacement to be small. In this approach, the necessary and sufficient condition of instability in our problem can be presented as (see Appendix B)

$$\left(\int dE \right)^{-1} \left[\int \frac{dE}{\lambda} \frac{u_0}{c_T} \right]^2 + \int \frac{dE}{\lambda^2} \left(1 - \frac{u_0^2}{c_T^2} + \frac{\lambda^2}{h^2} \right) < 0, \quad (38)$$

where $dE = dr r \sigma_0 |\xi|^2$; ξ is the radial gas displacement; λ is the characteristic space scale of perturbation change. For inequality (38) to be satisfied it is necessary that the first term, giving positive contribution, be small enough and the second term be negative. The last condition is met if the scale of change of perturbations is smaller than the disk thickness (this is one of the adopted by us conditions of developed turbulence) and if the radial velocity in a sufficiently large region of the disk is supersonic. The first condition is met if the radial motion in the disk is absent or the mean value of the radial velocity over the disk is close to zero, i.e. the velocity changes the sign. In other terms, the velocity should take higher values and should have a large gradient over sufficiently extended part of the disk. Both these conditions are satisfied in the present problem (see Appendix B).

The behavior of modes near the zero radial velocity points and the dispersion equation (37) are sufficient in principle to explain many properties of unstable perturbations presented in

Fig. 6. If in the inner part of the disk, restricted by the precessional wave, the radial velocity experiences a large gradient, local unstable modes arise. In the fourth quadrant of the disk the velocity gradient is not too high, and additionally the alternating in sign character of the velocity is less pronounced, so that the unstable modes are suppressed. The sub-Keplerian gas rotation in this region (see Fig. 3) also has the stabilizing effect. At the precessional wave boundary, as shown above, the perturbation amplitude vanishes. The amplitude increase in the outer parts of the disk, in the first and forth quadrants, can be due to the boundary effects³.

The physical sense of this instability can be explained as follows. In the radial Euler equation, the term with the background velocity gradient acts on the gas element as an external force, in addition to the pressure gradient force and centrifugal force. In our setting, the rotational flow has stabilizing effect and together with pressure prevents the instability development (both corresponding terms give positive contribution under the square root in (37)). However, if the velocity gradient is sufficiently high, the momentum flux transmitted to a perturbation due to this term can exceed the counter-acting contribution from stabilizing terms. According to (37), this condition occurs when the background radial velocity change on the scale of the perturbation length is approximately equal to or greater than the sound speed. In this case it is possible to argue that the rear phase of the perturbation catches up with its front phase in one wave period. Here the amplitude of perturbation maxima increases by the mass conservation. In terms of the dispersion relation, this signals the arising of non-zero values of the perturbation growth increment.

It should be noted once again that in our method of the instability analysis we assume axially symmetric perturbations, while the background density and velocity distributions do not have axial symmetry and weakly depend on the angle with the characteristic angular scale 2π (see Fig. 2). In a real disk, perturbations with this or smaller angular scale will shift in the tangential direction due to the background rotation. This could weaken the perturbation growth, which is due to the radial velocity gradient. However, the adopted here necessary condition for the turbulence to appear (25) requires that the characteristic growth time of perturbations be shorter than the Keplerian time. Thus, a perturbation in its growth time cannot leave the region of the precessional wave in the tangential direction and, hence, we observe the instability growth.

In Section 3, we applied the necessary conditions of three-dimensional turbulence development (25) to unstable modes. In the inner part of the disk, where the angular frequency of the gas is high, the conditions for the turbulence development are more stringent. They become favorable only in the outer part of the disk and near the zero radial velocity line, where the local wavelength of perturbations decreases.

Thus, the turbulence arising in the disk can be described as follows. Perturbations that have time to grow up to non-linear stage in less than one disk revolution and whose wavelength does not exceed the disk semi-thickness serve as sources for three-dimensional turbulence. The turbulence arises predominantly along the precessional wave boundary and beyond its outer edge and then is brought by the gas rotation and accretion flow over the entire disk.

5 Conclusion

Thin Keplerian disks are known to be stable against fluid perturbations [5, 6]. For a hydrodynamic instability to arise, it is necessary that the density and velocity distributions in the disk differ from the Keplerian ones [6]. The accretion disk in axially asymmetric gravitational

³Perturbations vanish at the calculation domain, but at the same time the eigenvectors of the problem (20) have a fixed norm, therefore in narrow regions, where there are favorable conditions for the instability development, the perturbation amplitude can be relatively high.

field of a binary stellar system provides an obvious example of such a configuration. In paper [34] we have shown that the gravitational field of the secondary binary component excites the precessional wave in the disk. The wave significantly changes the flow in the disk causing the appearance of regions with large density and velocity gradients. In the presented solution, the radial velocity gradient can be as high as 40 Machs.

In the present paper, we performed linear analysis of perturbations to study the stability of an isothermal accretion disk with precessional wave. The numerical model of the accretion disk in a binary system obtained in [34] was taken as the unperturbed background solution. The problem of linear perturbations growth was formulated in two dimensions in the inertial frame, where the precessional wave can be considered as stationary. The gas flow perturbations due to time-dependent gravitational field of the secondary component can be considered small. The strong twisting of the precessional wave allowed us to make linear analysis of radial perturbations only for each radial cut of the disk.

It was shown that the presence of the precessional wave gives rise to unstable radial modes with increments up to $\sim 50/P_{\text{orb}}$. However, for turbulence development, the presence of background regions with large radial velocity gradients is essential. The instability arises if the radial velocity change in the unperturbed flow on the wavelength of a perturbation is of the order of or greater than the sound speed. The physical reason of the instability is that the rear phase of the perturbation starts catching up with the frontal phase, which causes, by the mass conservation, the growth of the perturbation maxima amplitudes. The necessary conditions for turbulence (the wavelength smaller than the disk thickness, the increment exceeds the rotation frequency) are fulfilled only at the precessional wave boundaries and in the outer part of the disk.

The results of the present analysis suggest that the precessional wave in the disk can lead to turbulence with the characteristic Shakura-Sunyaev α -parameter of about 0.01.

The authors thank Yu.M. Torgashin and E.V. Polyachenko for valuable notes. We also thank the referee, P.B. Ivanov, for important notes and comments that helped improving the paper.

The work was supported by the Program of fundamental researches of the Presidium of RAS P-21 and P-22, by Russian Foundation for Basic Researches (projects 12-02-00047, 12-07-00528a, 13-02-00077) and the Program of support of leading scientific schools of RF.

6 Appendix A

The method of solving linearized equations we used in the present paper ignores the angular dependence of the background variables. This approach is different from the ordinarily used spectral method (see, for example, [36]), and its formulation is not fully rigorous. To show this, expand the system (11) in the basis of some functions of the angular coordinate. Conditionally determine the functional transformations in the form:

$$\tilde{f}(m) = \sum_{\phi} \Phi(\phi, m) f(\phi), \quad (39)$$

$$f(\phi) = \sum_m \Psi(\phi, m) \tilde{f}(m), \quad (40)$$

where $\{\Phi(\phi, m)\}$ and $\{\Psi(\phi, m)\}$ are mutually dual sets of functions depending on the angle ϕ and the parameter m . Thus expanded system (11) takes the form

$$\sum_{\beta=1}^3 \sum_{\phi', m'} \Phi(\phi', m) A_{\alpha\beta}(r, \phi') \Psi(\phi', m') \tilde{f}_{\beta}(r, m') = i\omega \sum_{\phi', m'} \Phi(\phi', m) \Psi(\phi', m') \tilde{f}_{\alpha}(r, m'). \quad (41)$$

In the ‘standard’ approach, the expansion is doing in the orthogonal set of functions, i.e. $\int d\phi' \Phi(\phi', m) \Psi(\phi', m') = 0$ for $m \neq m'$. In particular, this is valid for $\Phi(\phi', m) \propto e^{-im\phi'}$ and $\Psi(\phi', m') \propto e^{im'\phi'}$. The approach proposed in the present paper relies on an expansion in two harmonics only, which we denote as $m \equiv M$ and $m' \equiv 0$; here the orthogonality of functions is not assumed. Expansion (12) can be obtained if we define

$$\Phi(\phi', M) = \delta_D(\phi' - \phi) , \quad (42)$$

$$\Psi(\phi', 0) \equiv 1 . \quad (43)$$

where δ_D is the Dirac delta-function. In this case equations (39) and (40) take the form $\tilde{f}(0) = f(\phi)$.

It is seen that $\Psi(\phi', 0)$ represents an axially symmetric harmonic and the operator $\int d\phi' \Phi(\phi', M)$ ‘cuts’ the given direction in the disk. One of the assumptions of this approach is as follows. Although the expansion of the system (11) in non-orthogonal set of functions is quite admissible, one cannot be sure that functions (42) and (43) belong to two mutually dual sets in the sense of definitions (39) and (40) for *all* ϕ from 0 to 2π . Despite this fact, we prefer this method since it offers a more clear physical interpretation of the perturbation growth as a function of the background variables distribution because it provides the angular coordinate locality. Another assumption is that the proposed approach assumes the use of axially symmetric modes, whereas the background solution do depends on the angle. The distributions shown in Fig. 2 demonstrate that the main angular scale of changes is 2π . Therefore, this scale should mainly contribute in perturbations, and in the standard approach this scale would correspond to the azimuthal number $m = 1$. However, for simplicity we assume that the perturbation is axially symmetric. Thus, the problem can be formulated irrespective of each radial direction in the disk.

7 Appendix B

Below we briefly describe the instability analysis in the disk following to the Lynden-Bell-Ostriker’s method. A detailed presentation of the method and examples for axially symmetric flows can be found in paper [50].

The gas-dynamic equations can be written through the displacement vector of gas $\boldsymbol{\xi}$ relative to its equilibrium position (marked with index ‘0’):

$$\left(\frac{\partial}{\partial t} + \mathbf{V}_0 \nabla \right)^2 \boldsymbol{\xi} = -\Delta (c_T^2 \nabla \ln \sigma + \nabla \Phi) , \quad (44)$$

where Δ is the Lagrangian difference operator determined as

$$\Delta f = f(t, \mathbf{r} + \boldsymbol{\xi}(t, \mathbf{r})) - f_0(t, \mathbf{r}) = \quad (45)$$

$$= f(t, \mathbf{r}) - f_0(t, \mathbf{r}) + \boldsymbol{\xi}(t, \mathbf{r}) \nabla f_0(t, \mathbf{r}) + \mathcal{O}(|\boldsymbol{\xi}|^2) . \quad (46)$$

equation (44) should be supplemented with the continuity equation:

$$\Delta \sigma + \sigma_0 \nabla \boldsymbol{\xi} = 0 . \quad (47)$$

Further analysis is performed by assuming that the displacement is small and the unperturbed disk is steady. Let us define the displacement vector as $\boldsymbol{\xi} \mapsto e^{i\omega t} \boldsymbol{\xi}$. The linearized dynamical equations have the form

$$-\omega^2 \mathbf{A} \boldsymbol{\xi} + \omega \mathbf{B} \boldsymbol{\xi} + \mathbf{C} \boldsymbol{\xi} = 0 , \quad (48)$$

where \mathbf{A} , \mathbf{B} , and \mathbf{C} are matrices composed of the unperturbed variables and their derivatives. After multiplying this equation by vector $\boldsymbol{\xi}^+$ and integrating over the volume, we finally obtain the quadratic equation for ω :

$$-\omega^2 \int d^2r \boldsymbol{\xi}^+ \mathbf{A} \boldsymbol{\xi} + \omega \int d^2r \boldsymbol{\xi}^+ \mathbf{B} \boldsymbol{\xi} + \int d^2r \boldsymbol{\xi}^+ \mathbf{C} \boldsymbol{\xi} = 0 \quad (49)$$

or

$$-\omega^2 a + \omega b + c = 0 . \quad (50)$$

The necessary and sufficient condition for a linear perturbation to grow is the condition for the discriminant of this equation:

$$b^2 + 4ac < 0 . \quad (51)$$

In our problem, the displacement vector $\boldsymbol{\xi}$ contains only the radial component, and coefficients a , b и c have the form [50]

$$a = \int dr r \sigma_0 |\xi|^2 , \quad (52)$$

$$b = i \int dr r \sigma_0 \left(\xi^* \frac{d\xi}{dr} - \xi \frac{d\xi^*}{dr} \right) u_0 , \quad (53)$$

$$c = t + v + p ,$$

$$t = \int dr r \sigma_0 \left(-u_0^2 \left| \frac{d\xi}{dr} \right|^2 + 3\Omega_0 |\xi|^2 \right) , \quad (54)$$

$$v = \int dr r \sigma_0 |\xi|^2 \frac{d(r\Omega_K^2)}{dr} , \quad (55)$$

$$p = c_T^2 \int dr r \sigma_0 \left| \frac{d\xi}{dr} \right|^2 . \quad (56)$$

Using the equilibrium flow equation

$$c_T^2 \frac{d \ln \sigma_0}{dr} + r\Omega_K^2 - r\Omega_0^2 = 0 \quad (57)$$

and the disk semi-thickness in the form $h = c_T/\Omega_K$, the instability growth condition can be written as

$$\begin{aligned} & \left(\int dr r \sigma_0 |\xi|^2 \right)^{-1} \left[\int dr r \sigma_0 \operatorname{Im} \left(\xi \frac{d\xi^*}{dr} \right) \frac{u_0}{c_T} \right]^2 + \\ & + \int dr r \sigma_0 \left| \frac{d\xi}{dr} \right|^2 \left(1 - \frac{u_0^2}{c_T^2} \right) + \\ & + \int dr r \sigma_0 |\xi|^2 \left(\frac{1}{h^2} + \frac{1}{r} \frac{d \ln \sigma_0}{dr} \right) < 0 . \end{aligned} \quad (58)$$

Using (57) it is easy to show in the particular case where the fluid is incompressible and the radial flow is absent, expression (58) turns into the classical Rayleigh criterion [6]:

$$\int dr r \sigma_0 |\xi|^2 \kappa_0^2 < 0 . \quad (59)$$

The integrand in the first term of inequality (58) is the product of the radial velocity and a function whose scale of change corresponds to the given mode change scale. Indeed, equation (47) for the displacement ξ can be written as

$$\frac{d\xi}{dr} + \frac{d \ln(r\sigma_0)}{dr} \xi + \delta = 0 , \quad (60)$$

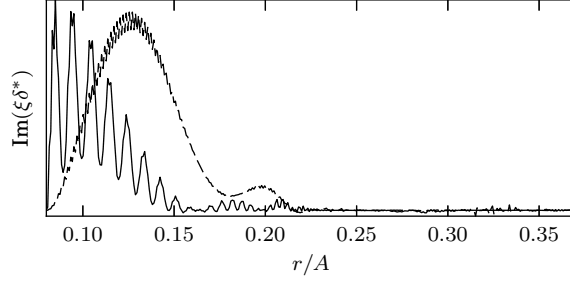


Figure 7: The value of $\text{Im}(\xi\delta^*)$ as a function of the radial disk coordinate for two modes shown in the left panel of Fig. 5 (see Appendix B).

from where it follows that $\text{Im}(\xi d\xi^*/dr) = -\text{Im}(\xi\delta^*)$. The plot of this function for two modes is presented in Fig. 7. By comparing these modes with those shown in Fig. 5 we conclude that the characteristic scale of change of these functions is the same, although functions $\text{Im}(\xi d\xi^*/dr)$ apparently do not change the sign. Oppositely, the radial velocity distribution changes the sign. Let us define the local scale of perturbation change λ as $\text{Im}(\xi d\xi^*/dr) \equiv \lambda^{-1}|\xi|^2$. As the background distribution change scale is larger than the scale of perturbations of interest here, the estimate $|d\xi/dr|^2 \simeq \lambda^{-2}|\xi|^2$. For the same reason we can neglect the density gradient in the last term of the l.h.s. of (58). Then the inequality takes the form

$$\left(\int dE\right)^{-1} \left[\int \frac{dE}{\lambda} \frac{u_0}{c_T}\right]^2 + \int \frac{dE}{\lambda^2} \left(1 - \frac{u_0^2}{c_T^2} + \frac{\lambda^2}{h^2}\right) < 0, \quad (61)$$

where $dE = dr r \sigma_0 |\xi|^2$. The numerical check of inequality (61) that we did also confirms the presence of instability. For example, for modes shown in Fig. 5 the typical value of the discriminant $1 + 4ac/b^2$ is of the order of -1 .

References

- [1] N. I. Shakura. Disk Model of Gas Accretion on a Relativistic Star in a Close Binary System. *Astron. Zh.*, 49:921, October 1972.
- [2] N. I. Shakura and R. A. Sunyaev. Black holes in binary systems. Observational appearance. *Astron. and Astrophys.*, 24:337–355, 1973.
- [3] D. Lynden-Bell and J. E. Pringle. The evolution of viscous discs and the origin of the nebular variables. *Mon. Not. R. Astron. Soc.*, 168:603–637, September 1974.
- [4] N. I. Shakura. Academician Zeldovich and the foundations of disk accretion. *Phys. Usp.*, 57:407–412, 2014.
- [5] P. Godon and M. Livio. On the Nonlinear Hydrodynamic Stability of Thin Keplerian Disks. *Astrophys. J.*, 521:319–327, August 1999.
- [6] S. A. Balbus, J. F. Hawley, and J. M. Stone. Nonlinear Stability, Hydrodynamical Turbulence, and Transport in Disks. *Astrophys. J.*, 467:76, August 1996.
- [7] E. P. Velikhov. Stability of an Ideally Conducting Liquid Flowing Between Cylinders Rotating in a Magnetic Field. *JETP*, 36:1398–1404, 1959.
- [8] S. Chandrasekhar. The Stability of Non-Dissipative Couette Flow in Hydromagnetics. *Proceedings of the National Academy of Science*, 46:253–257, February 1960.
- [9] S. A. Balbus and J. F. Hawley. A powerful local shear instability in weakly magnetized disks. I - Linear analysis. II - Nonlinear evolution. *Astrophys. J.*, 376:214–233, July 1991.
- [10] O. Regev. The Magneto-Rotational Instability Near Threshold: Spatio-Temporal Amplitude Equation and Saturation. In M. Goupil, Z. Koláth, N. Nardetto, and P. Kervella, editors, *EAS Publications Series*, volume 38 of *EAS Publications Series*, pages 165–173, 2009.
- [11] E. Liverts, Y. Shtemler, M. Mond, O. M. Umurhan, and D. V. Bisikalo. Nondissipative Saturation of the Magnetorotational Instability in Thin Disks. *Phys. Rev. Lett.*, 109(22):224501, November 2012.
- [12] A. M. Fridman and D. V. Bisikalo. The nature of accretion disks of close binary stars: overreflection instability and developed turbulence. *Phys. Usp.*, 51(6):551–576, June 2008.
- [13] W. Cabot. The nonaxisymmetric baroclinic instability in thin accretion disks. *Astrophys. J.*, 277:806–812, February 1984.
- [14] H. H. Klahr and P. Bodenheimer. Turbulence in Accretion Disks: Vorticity Generation and Angular Momentum Transport via the Global Baroclinic Instability. *Astrophys. J.*, 582:869–892, January 2003.
- [15] B. Mukhopadhyay and A. K. Chattopadhyay. Stochastically driven instability in rotating shear flows. *Journal of Physics A Mathematical General*, 46(3):035501, January 2013.
- [16] Y. E. Lyubarskij, K. A. Postnov, and M. E. Prokhorov. Eccentric Accretion Disks. *Mon. Not. R. Astron. Soc.*, 266:583, February 1994.
- [17] K. Sawada, T. Matsuda, and I. Hachisu. Spiral shocks on a Roche lobe overflow in a semi-detached binary system. *Mon. Not. R. Astron. Soc.*, 219:75–88, March 1986.

- [18] K. Sawada, T. Matsuda, and I. Hachisu. Accretion shocks in a close binary system. *Mon. Not. R. Astron. Soc.*, 221:679–686, August 1986.
- [19] K. Sawada, T. Matsuda, M. Inoue, and I. Hachisu. Is the standard accretion disc model invulnerable? *Mon. Not. R. Astron. Soc.*, 224:307–322, January 1987.
- [20] D. V. Bisikalo, A. A. Boyarchuk, O. V. Kuznetsov, and V. M. Chechyotkin. Three-dimensional modeling of the matter flow structure in semidetached binary systems. *Astron. Rep.*, 41:786–793, November 1997.
- [21] D. V. Bisikalo, A. A. Boyarchuk, O. V. Kuznetsov, and V. M. Chechetkin. Influence of a binary system common envelope on mass transfer through the inner Lagrange point. *Astron. Rep.*, 41:794–801, November 1997.
- [22] D. V. Bisikalo, A. A. Boyarchuk, O. A. Kuznetsov, and V. M. Chechetkin. The influence of parameters on the flow structure in semidetached binary systems: 3-D numerical modeling. *Astron. Rep.*, 42:621–629, September 1998.
- [23] D. V. Bisikalo, A. A. Boyarchuk, V. M. Chechetkin, O. A. Kuznetsov, and D. Molteni. Three-dimensional numerical simulation of gaseous flow structure in semidetached binaries. *Mon. Not. R. Astron. Soc.*, 300:39–48, October 1998.
- [24] D. V. Bisikalo, A. A. Boyarchuk, O. A. Kuznetsov, and V. M. Chechetkin. Three-dimensional modeling of mass transfer in close binary systems with asynchronous rotation. *Astron. Rep.*, 43:229–240, April 1999.
- [25] D. V. Bisikalo, A. A. Boyarchuk, O. A. Kuznetsov, and V. M. Chechetkin. Driven-disk model for binaries with a precessing donor star: Three-dimensional simulations. *Astron. Rep.*, 43:587–591, September 1999.
- [26] D. V. Bisikalo, A. A. Boyarchuk, V. M. Chechetkin, O. A. Kuznetsov, and D. Molteni. Comparisons of 2D and 3D simulations of mass transfer in semi-detached binaries. I. *Astron. Rep.*, 43:797–807, December 1999.
- [27] D. V. Bisikalo, A. A. Boyarchuk, O. A. Kuznetsov, and V. M. Chechetkin. The Effect of Viscosity on the Flow Morphology in Semidetached Binary Systems. Results of 3D Simulations. II. *Astron. Rep.*, 44:26–35, January 2000.
- [28] D. V. Bisikalo, P. Harmanec, A. A. Boyarchuk, O. A. Kuznetsov, and P. Hadrava. Circumstellar structures in the eclipsing binary β Lyr A. Gasdynamical modelling confronted with observations. *Astron. and Astrophys.*, 353:1009–1015, January 2000.
- [29] D. V. Bisikalo, A. A. Boyarchuk, A. A. Kil’Pio, O. A. Kuznetsov, and V. M. Chechetkin. The Structure of Matter Flows in Semi-Detached Binaries after the Termination of Mass Transfer. *Astron. Rep.*, 45:611–619, August 2001.
- [30] D. V. Bisikalo, A. A. Boyarchuk, A. A. Kilpio, and O. A. Kuznetsov. A possible manifestation of spiral shock waves in the accretion disks of cataclysmic variables. *Astron. Rep.*, 45:676–685, September 2001.
- [31] D. Molteni, O. A. Kuznetsov, D. V. Bisikalo, and A. A. Boyarchuk. On the angular momentum transfer on to compact stars in binary systems. *Mon. Not. R. Astron. Soc.*, 327:1103–1110, November 2001.

- [32] A. A. Boyarchuk, D. V. Bisikalo, O. A. Kuznetsov, and V. M. Chechetkin. *Mass transfer in close binary stars*. Taylor & Frances, London, 2002.
- [33] A. M. Fridman, A. A. Boyarchuk, D. V. Bisikalo, O. A. Kuznetsov, O. V. Khoruzhii, Y. M. Torgashin, and A. A. Kilpio. The collective mode and turbulent viscosity in accretion discs. *Physics Letters A*, 317:181–198, October 2003.
- [34] D. V. Bisikalo, A. A. Boyarchuk, P. V. Kaigorodov, O. A. Kuznetsov, and T. Matsuda. The Structure of Cool Accretion Disks in Semidetached Binaries. *Astron. Rep.*, 48:449–456, June 2004.
- [35] S. H. Lubow. A model for tidally driven eccentric instabilities in fluid disks. *Astrophys. J.*, 381:259–267, November 1991.
- [36] S. Kato. Resonant Excitation of Disk Oscillations in Deformed Disks II: A Model of High-Frequency QPOs. *Publications of the Astronomical Society of Japan*, 60:111–, February 2008.
- [37] S. Kumar. Twisted Accretion Disks - Part Two - Variation in Density Distribution and Application to Interacting Binaries. *Mon. Not. R. Astron. Soc.*, 223:225, November 1986.
- [38] B. Warner. *Cataclysmic Variable Stars*. Cambridge Univ. Press, Cambridge, 1995.
- [39] N. N. Gor’kavyj and A. M. Fridman. *Physics of planetary rings. Celestial mechanics of continuous medium*. Nauka, Moscow (Russia), 1994.
- [40] W. Kley, J. C. B. Papaloizou, and G. I. Ogilvie. Simulations of eccentric disks in close binary systems. *Astron. and Astrophys.*, 487:671–687, August 2008.
- [41] S. M. Churilov and I. G. Shukhman. On the Relation Between Volume and Surface Adiabatic Indices for Gaseous Subsystems of Flat Galaxies. *Astronomicheskij Tsirkulyar*, 1157:1, 1981.
- [42] A. M. Fridman and N. N. Gor’kavyj. *Physics of planetary rings*. Springer, New York, 1999.
- [43] A. M. Fridman and A. V. Khoperskov. *Physics of Galactic Disks*. Cambridge International Science Publishing Ltd, 2013.
- [44] H. Fisk Jonhson. An Improved Method for Computing a Discrete Hankel Transform. *Comp. Phys. Comm.*, 43:181–202, 1987.
- [45] E. Anderson, Z. Bai, C. Bischof, S. Blackford, J. Demmel, J. Dongarra, J. Du Croz, A. Greenbaum, S. Hammarling, A. McKenney, and D. Sorensen. *LAPACK Users’ Guide*. Society for Industrial and Applied Mathematics, Philadelphia, PA, third edition, 1999.
- [46] E. P. Kurbatov. *Mexican Hat wavelet in polar coordinates*. 2013.
- [47] N. M. Astaf’eva. Wavelet analysis: basic theory and some applications. *Phys. Usp.*, 39(11):1085–1108, 1996.
- [48] V. M. Canuto, I. Goldman, and O. Hubickyj. A formula for the Shakura-Sunyaev turbulent viscosity parameter. *Astrophys. J. (Lett.)*, 280:L55–L58, May 1984.
- [49] B. B. Kadomtsev. Plasma turbulence. In M. A. Leontovich, editor, *Review of plasma physics*, volume 4. Consultants Bureau (Plenum), New York (NY, USA), 1966.

- [50] D. Lynden-Bell and J. P. Ostriker. On the stability of differentially rotating bodies. *Mon. Not. R. Astron. Soc.*, 136:293, 1967.